

Accurate Electronic and Optical Properties of Organic Doublet Radicals Using Machine Learned Range-Separated Functionals

Cheng-Wei Ju,^{†,‡} Yili Shen,^{¶,§} Ethan J. French,^{†,||} Jun Yi,[†] Hongshan Bi,[†] Aaron
Tian,^{†,⊥} and Zhou Lin^{*,†}

[†]*Department of Chemistry, University of Massachusetts, Amherst, MA 01003, United
States*

[‡]*Pritzker School of Molecular Engineering, The University of Chicago, Chicago, IL, 60637,
United States*

[¶]*Manning College of Information and Computer Sciences, University of Massachusetts,
Amherst, MA 01003, United States*

[§]*College of Software Engineering, Tongji University, Yangpu, Shanghai 200092, China*

^{||}*Department of Mathematics and Statistics, University of Massachusetts, Amherst, MA
01003, United States*

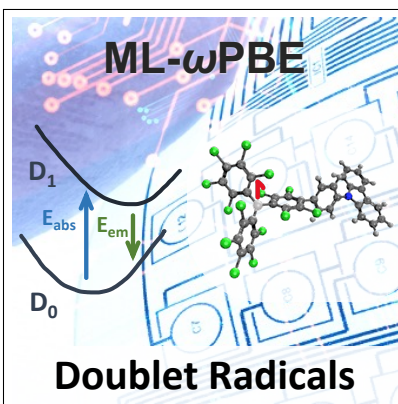
[⊥]*Massachusetts Academy of Math and Science, Worcester, MA, 01605, United States*

E-mail: zhoulin@umass.edu

Abstract

Luminescent organic semiconducting doublet-spin radicals are unique and emergent optical materials because their fluorescent quantum yields (Φ_{fl}) are not compromised by spin-flipping intersystem crossing (ISC) into any dark high-spin states. The multi-configuration nature of these radicals challenge their electronic structure calculations in the framework of single-reference density functional theory (DFT) and introduce room for method improvement. In the present study, we extend our earlier development of ML- ω PBE, a range-separated hybrid (RSH) exchange–correlation (XC) functional constructed using the stacked ensemble machine learning (SEML) algorithm, from closed-shell molecules to doublet-spin radicals. We assess its performance for an external test set of 64 radicals from five categories based on the original training set of 3,926 molecules. Interestingly, ML- ω PBE agrees with the first-principles OT- ω PBE functional regarding the molecule-dependent range-separation parameter (ω), with a small mean absolute error (MAE) of $0.0197 a_0^{-1}$ but saves the computational cost by 2.46 orders of magnitude. This result demonstrates outstanding generalizability and transferability of ML- ω PBE among various organic semiconducting species. To further assess the predictive power of ML- ω PBE, we also compare its performance on absorption and fluorescence energies (E_{abs} and E_{fl}) evaluated using time-dependent DFT (TDDFT), with nine conventional functionals. For most radicals, ML- ω PBE reproduces experimental measurements of E_{abs} and E_{fl} with small MAEs of 0.222 and 0.121 eV, only marginally different from OT- ω PBE. Our work illustrates a successful extension of the SEML framework from closed-shell molecules to open-shell radicals and will open the venue for calculating optical properties using single-reference TDDFT.

Graphical TOC Entry



An organic semiconducting doublet-spin radical can stabilize its unpaired electron through the delocalized π -conjugation and exhibit a non-conventional non-Aufbau configuration where the singly occupied molecular orbital (SOMO) is lower-lying than the highest (doubly) occupied molecular orbital (HOMO).¹⁻¹⁰ Such a long-lived open-shell configuration and the resulting compelling physicochemical characteristics, especially controllable optical properties between the doublet ground (D_0) and excited states ($D_{n>0}$), make it promising functional material for emergent scientific fields. For example, in photothermal therapy (PTT), the radical anion of a supramolecular complex of benzodithiophene-fused perylene diimide (BPDI) and cucurbit[7]uril (CB[7]) absorbs biologically transparent near-infrared (NIR) light and dissipates the photon energy as heat.¹¹⁻¹⁵ In organic light-emitting diodes (OLEDs), the D_1 state can reach a 100% fluorescent quantum yield (Φ_f) because it does not undergo any easy intersystem crossing (ISC) into a high-spin dark state.^{4,7,16-18}

However, due to the open-shell character of such an organic semiconducting radical, its electronic structures and optical properties are challenging to calculate.¹⁹ To address this problem while considering the molecular size, many multiconfiguration approaches have been developed based on density functional theory (DFT) and time-dependent density functional theory (TDDFT) and have been proven physically correct and reliable, including multi-configuration pair DFT (MC-PDFT),²⁰⁻²² spin-adapted TDDFT (X-TDDFT),²³⁻²⁶ spin-flip TDDFT (SF-TDDFT),²⁷⁻²⁹ and orbital optimization DFT (OODFT).³⁰⁻³² However, their applications have been limited to small and simple systems because of the difficulty in selecting and handling appropriate active spaces and electronic configurations without prior knowledge of the system, as well as the less friendly computational cost ($\simeq N_{\text{act}}N_{\text{orb}}^4$).³³⁻³⁵

The low computational cost ($\simeq N_{\text{orb}}^3$) and the black-box character make regular single-reference DFT and TDDFT appealing again for organic semiconducting radicals despite the theoretical challenge and the lack of reliable benchmarks. They can generate electronic structures and optical properties of these radicals to desired accuracy after careful development and calibration of exchange–correlation (XC) functionals.^{23,24,36-43} Head-Gordon and

coworkers performed systematic studies for excited state properties of polycyclic aromatic hydrocarbon (PAH) radical ions^{38,44–48} using original TDDFT and its simplified variant with Tamm–Dancoff approximation (TDA)⁴⁹ along with common functionals like BLYP^{50,51} and B3LYP.^{50–52} They found that TDDFT and TDDFT/TDA both reproduced experimental excited state energies with errors smaller than 0.3 eV when the basis set was reasonably large, in spite of the inexact XC functionals and adiabatic approximations and the inability to treat double excitations,^{53,54} and TDDFT/TDA outperformed TDDFT in capturing correct states by overcoming some orbital instability problems.^{49,55–59} They also assigned the strongest absorption of these radicals to involve their SOMOs. Other researchers, such as Joblin,^{39,60–62} Jacquemin,⁴¹ Grimme,^{63,64} Furche,^{65–67} and Allouche,⁶⁸ performed similar benchmark analyses on organic semiconducting radicals and obtained physical insights and reaction mechanisms. All these DFT-based studies have demonstrated the advantages of global hybrid (GH)^{50–52,69–77} or range-separated hybrid (RSH)^{78–89} functionals with molecule-dependent parameters for organic semiconducting radicals due to the necessity to balance the accuracy of electronic density in the short and long ranges.

Motivated by the urgent demand for a molecule-dependent RSH XC functional and the rapid advancement in machine learning (ML), we designed a new functional referred to as ML- ω PBE⁸⁹ based on a stacked ensemble machine learning (SEML) algorithm.^{90–95} We provide the detailed scheme in Figure S1 and Algorithm S1 in the Supporting Information (SI). In that study, we determined the molecule-dependent range-separation parameter (ω), defined in the separation of the Coulomb operator,

$$\frac{1}{|\mathbf{r} - \mathbf{r}'|} = \underbrace{\frac{1 - \text{erf}(\omega|\mathbf{r} - \mathbf{r}'|)}{|\mathbf{r} - \mathbf{r}'|}}_{\text{short range}} + \underbrace{\frac{\text{erf}(\omega|\mathbf{r} - \mathbf{r}'|)}{|\mathbf{r} - \mathbf{r}'|}}_{\text{long range}} \quad (1)$$

using a composite molecular descriptor (CMD)^{96–101} and a stacked generalization ideology. We systematically benchmarked ML- ω PBE using 3,926 organic semiconducting molecules in the same study. We compared the values of ω obtained from ML- ω PBE (ω_{ML}) with

those from OT- ω PBE (ω_{OT}), which optimally tunes the value of ω based on Koopmans’ theorem^{22,88,89,102–107} by minimizing the metrics of

$$J^2(\omega) = [\varepsilon_{\text{HOMO}}(\omega) + I(\omega)]^2 + [\varepsilon_{\text{LUMO}}(\omega) + A(\omega)]^2 \quad (2)$$

We proved that well-trained ML- ω PBE perfectly reproduces ω from OT- ω PBE with a mean absolute error (MAE) of 2.5%, but significantly reduces the computational cost by 2.66 orders of magnitude. We also compared ML- ω PBE-predicted optical properties with OT- ω PBE and many popular functionals,^{50–52,69,72,77,79,84,108,109} and found that ML- ω PBE reproduced the accuracy of OT- ω PBE and outperformed every other functional. It is worth noticing that the test set in that study includes some “external” molecules with *no* structural analogs present in the training set,^{88,110–112} and their successful treatments indicate advantages of our SEML model and ML- ω PBE that were seldom observed in other ML models and XC functionals, referred to as a substantial transferability or *domain adaption*.

In the present study, we assess the domain adaption of ML- ω PBE from closed-shell organic semiconducting molecules to doublet-spin organic semiconducting radicals (Figure 1) by asking whether these radicals can adopt the success of ML- ω PBE. Herein we constructed a brand new test set of 64 radicals, including 35 carbon-based radicals (C-1 through C-19 and C-49 through C-64),^{17,113–133} 2 PAH-based radicals (PAH-20 and PAH-21),^{134,135} 13 nitrogen-based radicals (N-22 through N-34),^{136–144} 6 nitrogen-oxygen-based radicals (NO-35 through NO-40),^{145–150} and 8 aryl oxygen-based radicals (ArO-41 through ArO-48).^{151–158} We provide their Cartesian (XYZ) coordinates for optimized D_0 and D_1 states of relevant species in the SI. We also combine all 3,926 molecules from the original training and test sets^{89,159–164} into the new training set. In the following sections, we will show that the absence of radical species from the training set does not undermine the predictive power of ML- ω PBE in ω , electronic structures, and optical properties. To describe the structural and electronic configurations for all these molecules and radicals, we construct their CMDs following the

same procedure as the earlier study.^{96,96-101} We revisit details about the training set and components for the CMD in the SI.

In the present study, we reapply the “top-down” SEML algorithm which implements the stacked generalization of eight successful descriptor-based regression models (or base learners).^{165,165-171} We select these regression models against the more popular neural networks (NNs) because they are less expensive, less data-demanding, and interestingly, sometimes more powerful. Their advantages become more significant when molecular and dataset sizes are larger.¹⁷²⁻¹⁷⁹ Also, earlier studies demonstrated that stacked generalization has a stronger predictive power than every single model.⁸⁹⁻⁹⁵ In our model, each base learner generates a non-linear quantitative relationship between the CMD the optimal ω_{ML} . A master least angle regression model (meta learner)¹⁸⁰ collects and analyzes all these relationships and produces the final prediction of ω_{ML} . We herein provide information about the base and meta learners in the SI too.

In the present study, we assess the performance of ML- ω PBE from a few different aspects. First, we confirm the capacity of ML- ω PBE in domain adaption by showing that the non-linear quantitative relationship between the CMD and ω_{ML} can be extrapolated from the domain of closed-shell molecules to that of doublet-spin radicals. In Figures 2(a) and (b), we compare the optimal values of ω_{OT} and ω_{ML} for the test set. Figure 2(a) shows that both ω_{OT} and ω_{ML} range broadly between 0.120 and 0.320 a_0^{-1} , which is similar to the range given by the training set⁸⁹ and indicates that it is appropriate to implement a system-dependent value of ω for an organic semiconducting radical rather than selecting a typical universal value. For example, the typical $\omega = 0.300 a_0^{-1}$ from LC- ω PBE⁸⁴ fails to capture correct electronic structures for our radicals for which optimal ω_{ML} and ω_{OT} are far from $\omega = 0.300 a_0^{-1}$. In addition, the average values $\langle \omega_{\text{OT}} \rangle = 0.178 a_0^{-1}$ and $\langle \omega_{\text{ML}} \rangle = 0.191 a_0^{-1}$ are lower than those of the training set ($\langle \omega_{\text{OT}} \rangle = 0.206 a_0^{-1}$), suggesting more diffuse and delocalized electronic structures from doublet-spin radicals. Figure 2(b) illustrates an excellent agreement between ω_{ML} and ω_{OT} , arriving at a small MAE of $\langle \Delta_{\text{ML}} \rangle = 0.0197 a_0^{-1}$ with a narrow distribution

of deviations. Among all 64 radicals, 33 exhibits absolute errors (AE) $\Delta_{\text{ML}} \leq \langle \Delta_{\text{ML}} \rangle$ and 27 gives $\Delta_{\text{ML}} \leq 2 \langle \Delta_{\text{ML}} \rangle$. Compared to the previous study,⁸⁹ the current $\langle \Delta_{\text{ML}} \rangle$ is more than three times as large. However, we can still claim the successful domain adaption of ML- ω PBE because (1) this value is only 11.1% of $\langle \omega_{\text{OT}} \rangle$ and 10.3% of $\langle \omega_{\text{ML}} \rangle$ and turns out not to affect the predictive power of ML- ω PBE and (2) there are only molecules but no radicals in the current training set. In addition, the computational time for generating ω ($\langle t_{\omega} \rangle$) is reduced from 63,442 seconds for OT- ω PBE to 221 seconds for ML- ω PBE, which is a substantial save by 2.46 orders of magnitude. This result proves that ML- ω PBE is as successful for radicals as for molecules, with comparable accuracy to OT- ω PBE but considerably higher efficiency.

Second, we explore the origin behind the successful domain adaption of ML- ω PBE. To analyze the chemical space occupied by the training and test sets, we illustrate the t-distributed stochastic neighbor embedding (t-SNE)¹⁸¹ in Figures 3(a) and S2. To extract important molecular representation features and validate the advantage of CMDs, we compare the performance of a simplified CMD constructed using ECFP4 (Morgan)^{97,182} and PaDEL¹⁸³ fingerprints (Figure 3) and the simple ECFP4 (Morgan) fingerprint (Figure S2). The t-SNE results demonstrate obviously that the features of radicals in the test set are highly diversified as long as the chemical space is described using an appropriate CMD, but their range significantly overlap with molecules from the training set. This observation partially deciphers the cause of successful domain adaption. Also, compared to the simple ECFP4 fingerprint, the t-distribution given by the simplified CMD shows a more substantial but not perfect natural clustering, validating a stronger capacity of differentiating molecules and indicating a room for improvement in molecular representations.¹⁸⁴⁻¹⁸⁸ As a further validation, Figure 3(b) compares the value of ω_{ML} for all radicals in the test set to their closed-shell hydrogenated counterparts (with an additional hydrogen atom added to the radical site), and shows that they are very close to each other with a tiny MAE of $0.00434 a_0^{-1}$. Such an extreme similarity proves that the molecular features extracted by our CMD and SEML model are so stable that similar electronic structures lead to similar predictions of ω_{ML} .

Third, before we systematically discuss the accuracy of ML- ω PBE on radical electronic structures, we will take a short detour and examine the sensitivity of electronic structures to the varying value of ω , as motivated by the insufficient benchmark of RSH functionals on open-shell systems. Figure 4(a) presents two representative molecules from the training set, including 2,2',2''-(2-phenylethene-1,1,2-triyl)trinaphthalene (AIE-16) with a locally excited (LE) singlet first excited state (S_1)^{89,110} and 2-phenyl-5-(4-(10-phenylphenazin-5(10H)-yl)phenyl)-1,3,4-oxadiazole (TADF-8) with a charge transfer (CT) S_1 state,^{89,112} as well as three representative radicals from the test set, including the carbon-based radicals (2',3',5',6'-tetrafluoro-N,N-diphenyl-4-amine-[1,1'-biphenyl])-(bis(perchlorophenyl))methyl (C-6) with a primarily CT D_1 state and tris(3,5-diisopropylphenyl)methyl (C-7) with a primarily LE D_1 state, and the nitrogen-based radical S-(2,4-dichlorophenyl)-N-(5'-phenyl-[1,1':3',1''-terphenyl]-2'-yl)thiohydroxylaminyl (N-23) with a partial CT D_1 character. For relevant species among the five, we illustrate their frontier molecular orbitals (MOs) evaluated using ML- ω PBE in Figures 4(b) and S3–S5. We also provide, as functions of ω between 0.050 and 0.400 a_0^{-1} , their energies associated with D_1 (E_{abs}) in Figure 4(c), total spin configurations ($\langle S^2 \rangle$) associated with D_0 and D_1 in Figure 4(d), and natural transition orbital (NTO) pairs associated with D_1 in Figures 4(e) and S12–S21 .

In our calculations, the change in the orbital configuration from β electrons to α electrons (Figure 4(b)) demonstrates the change in the electronic structures before and after introducing the unpaired electron. In addition to a universal significant energy decrease from an unoccupied SOMO to its occupied counterpart, SOMO, HOMO, and/or HOMO–1 of C-6 and N-23 also exhibit substantial re-ordered and mixed characters, or in other words *non-Aufbau* configuration, after involving the unpaired electron. For both radicals, β HOMO \rightarrow SOMO transitions dominate their D_1 states because their energy gaps are smaller than α HOMO–LUMO gaps, and limited spatial overlaps between MO and NTO pairs validate their CT and partial-CT characters. C-7, on the other hand, maintains its Aufbau configuration, but its D_1 gives a mixed transition of α SOMO \rightarrow LUMO and β HOMO \rightarrow SOMO because

of similar energy gaps. Significant spatial overlap between MO and NTO pairs confirms its LE character. These results endorse the possibility of vital change in orbital configuration when their occupations vary.

Figure 4(c) exhibits a bimodal relationship between E_{abs} and ω . For AIE-16, TADF-8, and N-23, E_{abs} monotonically increases with ω as expected, because the raised effective fraction of Hartree–Fock (HF) exchange over-localizes electrons and over-estimates E_{abs} .¹⁸⁹ Their leading NTO pairs remain similar across the broad range of ω , except that the fraction of the CT character monotonically decreases with an increasing ω , and small contributions (amplitude < 0.20) from other transitions might appear. On the contrary, C-6 and C-7 demonstrate non-monotonic trends in E_{abs} . They increase first with the rising ω , peak at $\omega = 0.310$ and $0.290 a_0^{-1}$, respectively, and decrease afterward. In addition to the ever-increasing localization of MOs, the NTO pairs also shift characters and become more complicated between 0.200 and $0.300 a_0^{-1}$. The spin configurations for C-6, C-7, and N-23 in Figure 4(d) further rationalize the mixing of NTOs. Although all of them present a universal increasing spin symmetry breakdown with an increasing fraction of HF exchange, neither D_0 nor D_1 of N-23 experiences a significant shift from an expected doublet ($\langle S^2 \rangle = 0.75$), while D_1 states of C-6 and C-7 experience more substantial mixing from quartets ($\langle S^2 \rangle > 1.50$) compared to D_0 . The notable breakdown of C-6 and C-7 agrees with the ever-increasing mixing character of NTO pairs and explains bimodal configurations for E_{abs} . The situation is exceptionally serious for C-6 because its NTO pairs are more delocalized and charge transferred. All discussions herein and later reveal an important reason for optimizing ω for radicals. Difficulty and instability are embedded in RSH functionals when applied to open-shell systems, making the subtle balance between over-delocalizing PBE and over-localizing HF important. In particular, the excited-state electronic structures of doublet-spin radicals are susceptible to the choice of ω , especially when they exhibit more delocalized or CT characters.

Finally, we will benchmark ML- ω PBE by examining its predictive power for E_{abs} and

the fluorescence energy (E_{fl}) of doublet-spin radicals in the test set. We construct the test subset for E_{abs} using C-1 to C-9, PAH-20 to PAH-21, N-22 to N-34, NO-35 to NO-40, and ArO-41 to ArO-48, and the test subset of E_{fl} using C-49 to C-64. We calculate E_{abs} and E_{fl} for relevant radicals using ML- ω PBE and different basis sets in the framework of linear response (LR) TDDFT with and without TDA, and compared their accuracy in terms of MAEs and/or mean signed errors (MSEs) with OT- ω PBE^{88,89} and seven other popular XC functionals, including LC- ω PBE with $\omega = 0.200 a_0^{-1}$ and $0.300 a_0^{-1}$,^{84,85} CAM-B3LYP,¹⁰⁹ ω B97X-D3,⁷⁹ M06-2X,⁷⁷ PBE,¹⁰⁸ PBE0,^{69,72} and B3LYP,⁵⁰⁻⁵² We provide all statistics in Figure 5 and Tables S1–S7 in the SI and draw a few conclusions about the outstanding performance of ML- ω PBE from these results. To begin with, we re-validate the above-mentioned high sensitivity of the accuracy of E_{abs} and E_{fl} to the choice of ω , especially for radicals with CT-like D_1 states like C-6. As expected earlier, the standard LC- ω PBE with $\omega = 0.300 a_0^{-1}$ shows a poor performance regardless of the choice of the TDDFT variant and the basis set, because $\omega = 0.300 a_0^{-1}$ is far from ω_{ML} for all radicals except for phenoxy (ArO-42). On the other hand, if we reduce ω to a value closer to $\langle\omega_{\text{OT}}\rangle = 0.178 a_0^{-1}$ and $\langle\omega_{\text{ML}}\rangle = 0.191 a_0^{-1}$, like $\omega = 0.200 a_0^{-1}$, LC- ω PBE improves its performance but does not reach consistently comparable MAEs and MSEs with ML- ω PBE and OT- ω PBE because its ω is fixed. This situation is particularly serious for large carbon-based radicals with significantly lower values of ω , such as 4'-(9H-carbazol-9-yl)-2,3,5,6-tetrachloro-[1,1'-biphenyl]-(bis(perchlorophenyl)methyl) (C-4) ($\omega_{\text{ML}} = 0.162 a_0^{-1}$) and tris(4-(9-butyl-9H-carbazol-3-yl)-2,3,5,6-tetrachlorophenyl)methyl (C-13) ($\omega_{\text{ML}} = 0.137 a_0^{-1}$). This re-validated sensitivity re-emphasizes the necessity to apply a system-dependent ω to organic semiconducting radicals.

Next, we will show that well-trained ML- ω PBE outperforms conventional functionals and accurately reproduces experimental optical properties. For the carbon-, PAH-, nitrogen, and nitrogen-oxide-based radicals in the E_{abs} test subset, ML- ω illustrates a distinct performance with an overall MAE of 0.222 eV and an overall MSE of +0.126 eV using TDDFT/6-311G(d),

being only marginally different from OT- ω PBE and exceeding all other functionals. Similar behavior is observed for carbon-based radicals in the E_{H} test subset. We attribute these achievements to the excellent agreement between ω_{ML} and ω_{OT} (Figure 2(b)), as well as the detailed balance between PBE and HF and between LE and CT, for most of the radicals in question. Further, this result re-implies the robustness of ML- ω PBE among distinct domains. In particular our CMD can precisely represent the features of these radicals and the SEMML algorithm can reliably construct a quantitative relationship between the CMD and ω_{ML} . To visualize our analysis, we compare the characters of frontier α MOs of C-4 generated by ML- ω PBE, every other functional and the *ab initio* complete active space configuration interaction (CASCI) approach (Figure 6). CASCI predicts an energy order of HOMO-1 < HOMO < SOMO for α electrons. ML- ω PBE with $\omega = 0.162 a_0^{-1}$, OT- ω PBE with $\omega = 0.173 a_0^{-1}$, and LC- ω PBE with $\omega = 0.200 a_0^{-1}$ slightly switch the order by giving HOMO-1 < SOMO < HOMO, while all other functionals considerably switch the order by giving SOMO < HOMO-1 < HOMO. This result justifies the importance of obtaining correct key electronic structures in predicting optical properties. Among the non-RSH functionals in comparison, the global hybrid PBE0^{69,72} with 75% PBE¹⁰⁸ and 25% HF appears to be an exception because it occasionally gives smaller MAEs and MSEs than ML- ω PBE and OT- ω PBE. This behavior is highly likely due to the error cancellation between D₀ and D₁. However, considering the re-ordered frontier MOs of C-4 reported by PBE0 (Figure 6), we conclude that a great energy agreement does not necessarily equal a great description of electronic structures.

In addition, the aryl oxygen-based radicals from the test set present poor reproduction of E_{abs} by underestimating it by more than 1 eV regardless of the choice of functional. We will show that this huge error originates from the incorrect or unstable electronic structures obtained from single-reference DFT and TDDFT. To showcase our idea, we select ArO-42, the smallest aryl oxygen-based radical and calculate its E_{abs} and four frontier MOs (HOMO-7, HOMO-1, HOMO, and SOMO) using ML- ω PBE, all other functionals in the

discussion, and *ab initio* CASSCF and CASCI approaches (Figure S11). Based on our analysis, the errors of E_{abs} obtained from all DFT methods are significantly greater than the benchmark CASSCF (10,7) calculations (-0.145 eV) due to the substantially re-ordered frontier MOs. For example, SOMO (# 25) predicted by CASSCF (10,7) represents a localized π_z bond between the oxygen atom and the carbon atom next to it. However, this orbital is split into HOMO-6 (# 18) and HOMO-2 (# 22) by ML- ω PBE ($\omega = 0.190 a_0^{-1}$) and OT- ω PBE ($\omega = 0.178 a_0^{-1}$). On the other hand, SOMO predicted by ML- ω PBE and OT- ω PBE represents a delocalized π_y^* bond at the same position but is originally HOMO-7 (# 17) from CASSCF (10,7). Frontier MOs from all of the rest functionals exhibit similar re-ordered behaviors. These results illustrate a fundamental problem in single-reference DFT, which can introduce serious errors to radicals with a localized unpaired electron, even after the most careful calibration of the XC functional. Herein we re-confirm the essence of obtaining correct electronic structures.

In the end, we compare the performance of ML- ω PBE across different combinations of TDDFT variants and basis sets. The basis set with diffuse functions, 6-311G+(d), does not improve the accuracy of ML- ω PBE because the critical MOs are not very delocalized. Figures S6-S8 present that frontier MOs of radicals occupy similar space to their hydrogenated counterparts or are slightly more localized. Also, the inclusion of TDA slightly compromises the accuracy of E_{abs} and E_{fl} , indicating that these radicals are less likely to suffer from the instability problems like some organic semiconducting molecules and it is necessary to include de-excitation and coupling matrices in the working eigenvalue equations of linear response.^{49,55-59}

In conclusion, we perform a follow-up assessment study for ML- ω PBE,⁸⁹ which was self-developed based on the top-down SEMML strategy,⁹⁰⁻⁹⁵ and expand its application domain from closed-shell singlet molecules¹⁵⁹⁻¹⁶⁴ to open-shell doublet radicals^{17,113-158} in the framework of single-reference DFT and TDDFT. Even with only closed-shell molecules in the training set, ML- ω PBE reproduces the molecule-dependent values of ω generated by

OT- ω PBE with a MAE of $0.0197 a_0^{-1}$ over all doublet radicals in the test set, but reduces the average computational cost by 2.46 orders of magnitude. Due to accurate captures of electronic structures, ML- ω PBE demonstrates an analogous top predictive power to OT- ω PBE regarding experimentally observable E_{abs} and E_{fl} for most radicals, and outperforms every other XC functionals in discussion^{50–52,69,72,77,79,84,108,109} without prominent error cancellations. The only exception is the aryl oxygen-based family for which all single-reference DFT methods fail to obtain correct energy orders of frontier MOs. In summary, through our study we validate and strengthen the practical value of ML- ω PBE in deciphering and predicting optical properties for luminescent organic semiconducting radicals and facilitate its application in large-scale computationally aided materials discovery for various emergent areas.

Acknowledgement

The authors would like to acknowledge the UMass/URI Unity Cluster and MIT Super-Cloud¹⁹⁰ for providing high-performance computing (HPC) resources. Z.L. would like to acknowledge UMass Amherst for providing the start-up funds to accomplish this study. Also, we would like to thank the helpful discussions with Prof. Hui Guan, Dr. Kun Yao, Dr. Lixue (Sherry) Cheng, Dr. Xin Chen, and Mr. Junjie Yang.

Supporting Information Available

The Supporting Information is available free of charge at XXXXXXXXXX.

- Details of quantum chemical calculations; brief revisit of the SEML model; similarity and difference in chemical space between molecules and radicals; error statistics of ML- ω PBE and other XC functionals in optical properties; and configurations of frontier MOs and NTOs (PDF).

- Optimized D_0 and D_1 geometries for relevant radicals in the external test set (ZIP).
- SMILES strings and ω values for all 64 radicals in the external test set (XLSX).

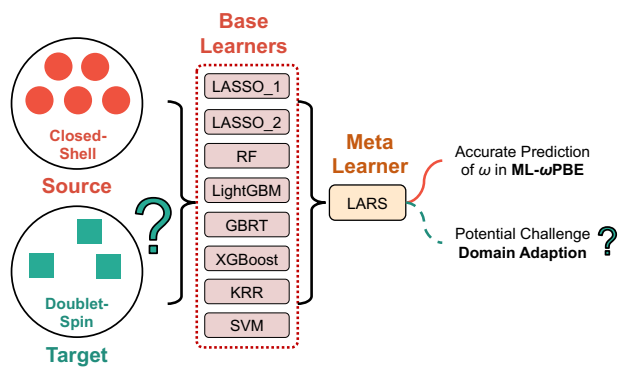


Figure 1: Architecture of SEML for ML- ω PBE and potential challenge in domain adaption from molecules to radicals.

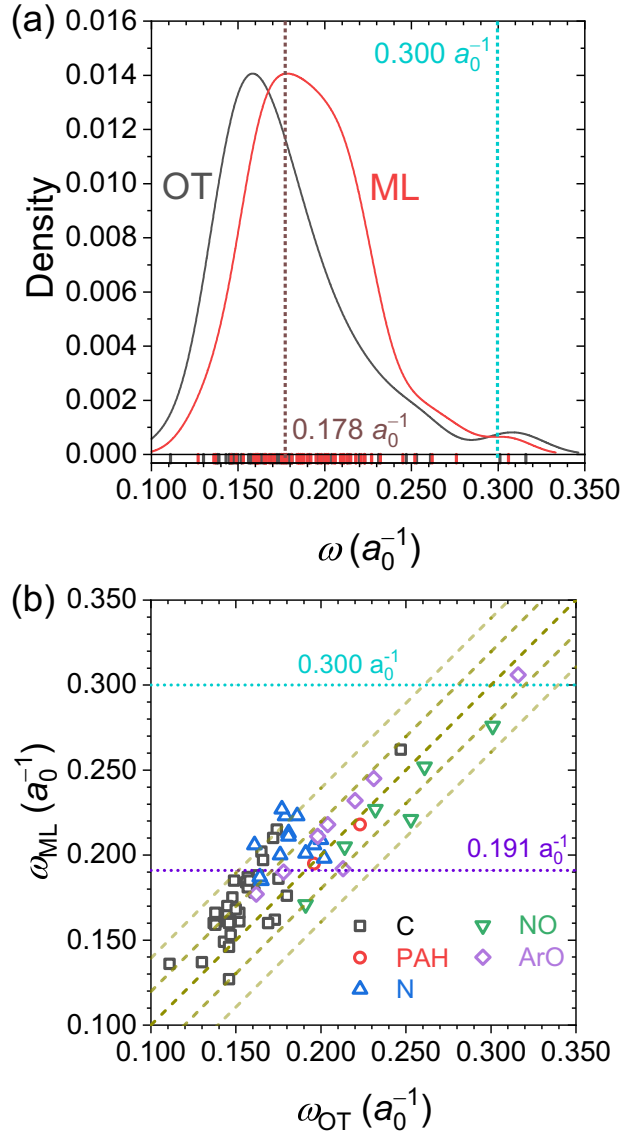


Figure 2: Comparison between ω_{ML} and ω_{OT} for all radicals are illustrated using (a) distribution and (b) scattered plots. Average $\langle\omega_{OT}\rangle = 0.178 a_0^{-1}$ and $\langle\omega_{ML}\rangle = 0.191 a_0^{-1}$ and the default $\omega = 0.300 a_0^{-1}$ are labeled using the dotted lines, and $\omega_{ML} - \omega_{OT} = 0, \pm\Delta\omega, \pm 2\Delta\omega$ are labeled using dashed lines.

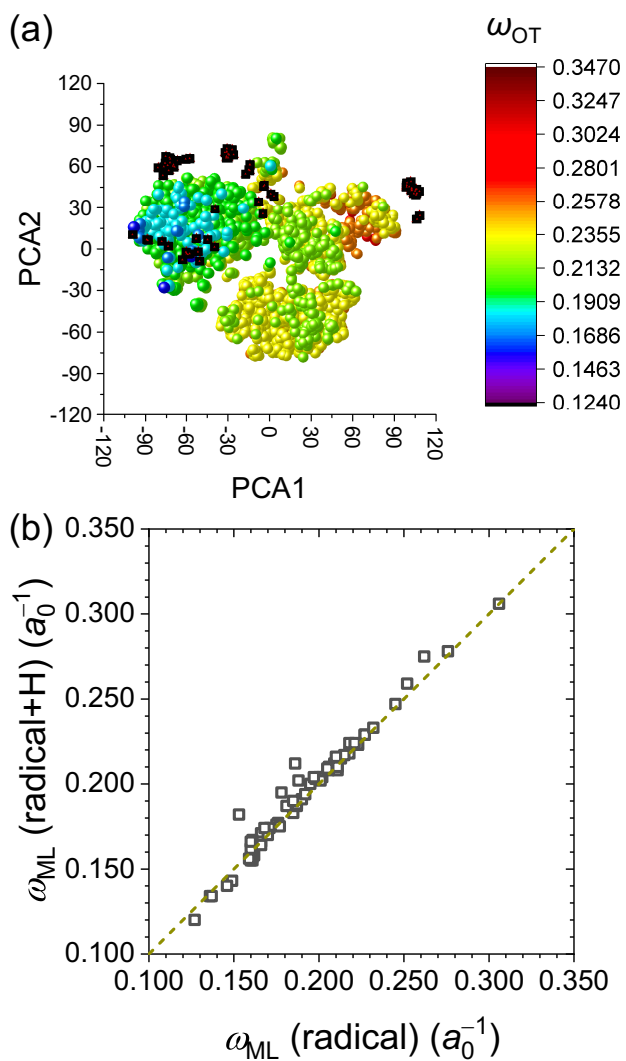


Figure 3: (a) t-SNE results on all molecules (colorful spheres), as well as all radicals (black cubes) and hydrogenated counterparts (red tetrahedrons) are described using the CMD from ECFP4 (Morgan)^{97,182} and PaDEL¹⁸³ fingerprints, with ω_{OT} represented using the color bar. (b) Comparison in ω_{ML} between radicals and hydrogenated counterparts.

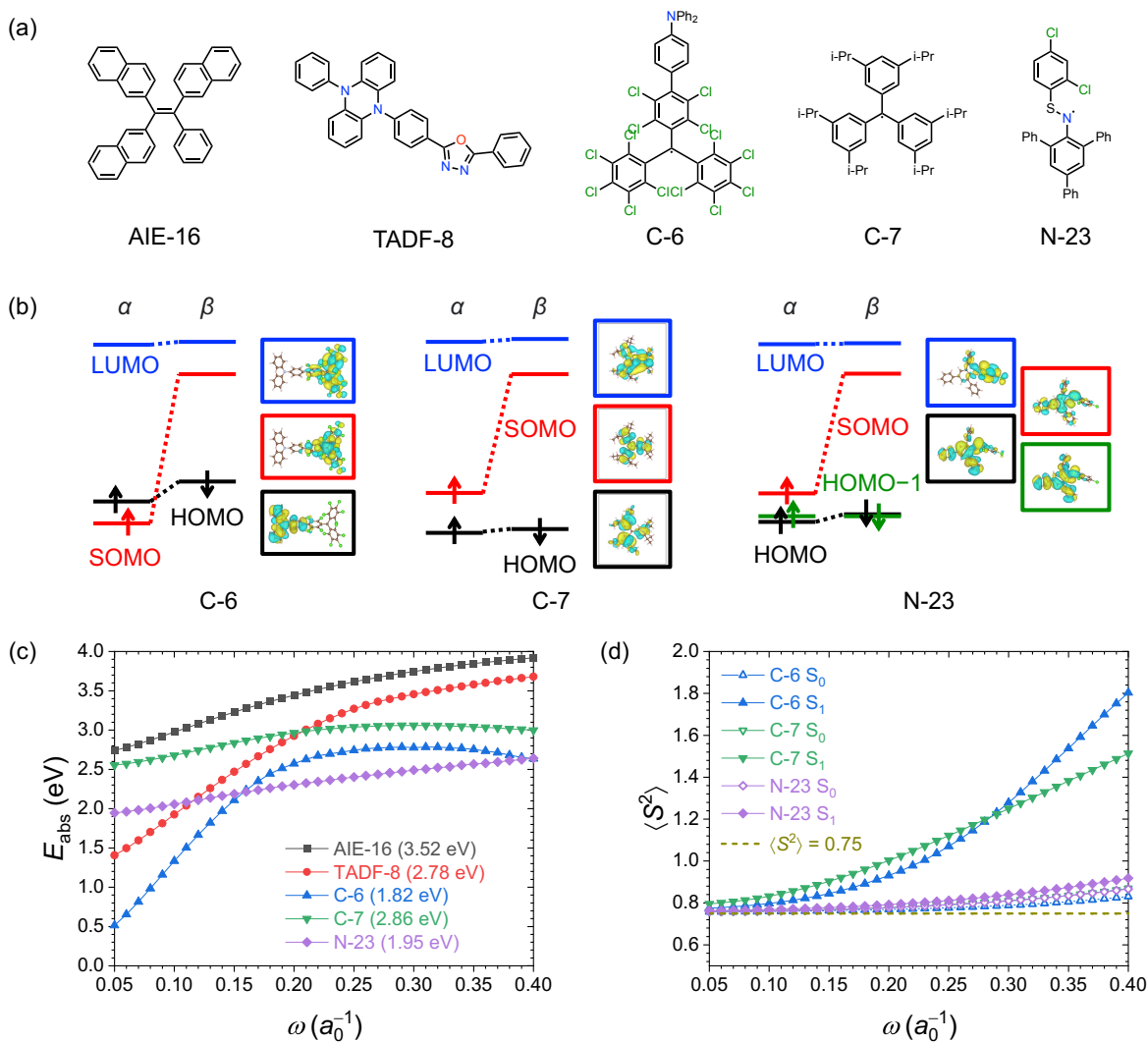


Figure 4: (a) Structures of AIE-16, TADF-8, C-6, C-7, and N-23. (b) Frontier MOs evaluated using ML- ω PBE. (c) Relationship between calculated E_{abs} (eV) and ω (a_0^{-1}), with experimental E_{abs} in the parentheses. (d) Relationship between calculated $\langle S^2 \rangle$ associated with D_0 and D_1 and ω (a_0^{-1}).

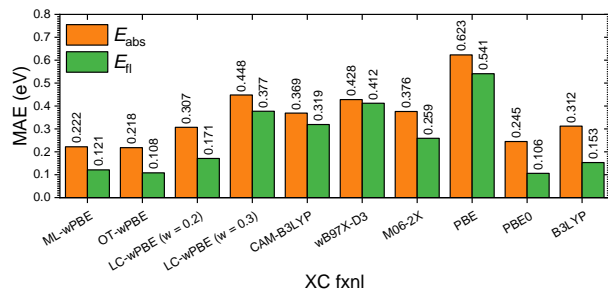


Figure 5: MAEs (eV) of E_{abs} and E_{fl} evaluated using ML- ω PBE and TDDFT/6-311G(d) for relevant radicals and compared with eight conventional XC functionals.

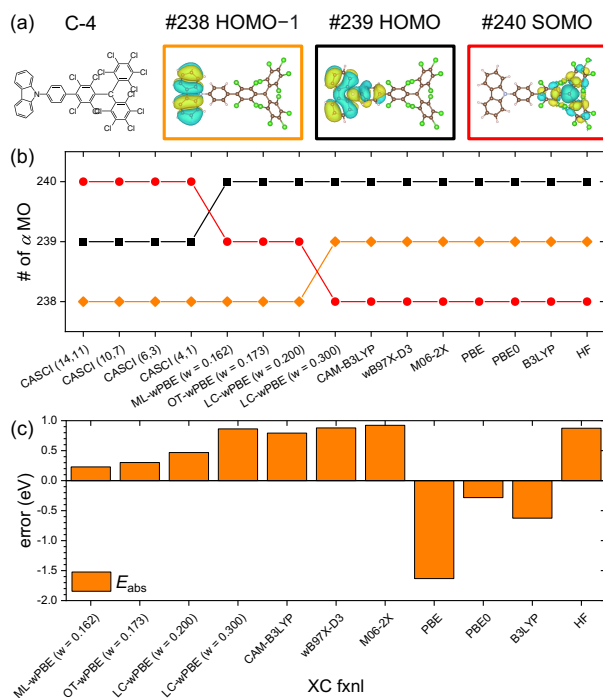


Figure 6: (a) HOMO-1 (orange), HOMO (black), and SOMO of C-4 evaluated using CASCI (14,11). (b) Ordering of α MOs of C-4 evaluated using various XC functionals to exhibit the leading characters of HOMO-1, HOMO, and SOMO as labeled in (a). (c) Signed errors (eV) of E_{abs}

References

- (1) Gryn'ova, G.; Marshall, D. L.; Blanksby, S. J.; Coote, M. L. Switching Radical Stability by pH-Induced Orbital Conversion. *Nat. Chem.* **2013**, *5*, 474–481.
- (2) Kumar, A.; Sevilla, M. D. SOMO–HOMO Level Inversion in Biologically Important Radicals. *J. Phys. Chem. B* **2018**, *122*, 98–105.
- (3) Reineke, S. Radically More Stable. *Nat. Mater.* **2019**, *18*, 917–918.
- (4) Guo, H.; Peng, Q.; Chen, X.-K.; Gu, Q.; Dong, S.; Evans, E. W.; Gillett, A. J.; Ai, X.; Zhang, M.; Credginton, D. et al. High Stability and Luminescence Efficiency in Donor–Acceptor Neutral Radicals not Following the Aufbau Principle. *Nat. Mater.* **2019**, *18*, 977–984.
- (5) Tanushi, A.; Kimura, S.; Kusamoto, T.; Tominaga, M.; Kitagawa, Y.; Nakano, M.; Nishihara, H. NIR Emission and Acid-Induced Intramolecular Electron Transfer Derived from a SOMO–HOMO Converted Non-Aufbau Electronic Structure. *J. Phys. Chem. C* **2019**, *123*, 4417–4423.
- (6) Cho, E.; Coropceanu, V.; Brédas, J.-L. Organic Neutral Radical Emitters: Impact of Chemical Substitution and Electronic-State Hybridization on the Luminescence Properties. *J. Am. Chem. Soc.* **2020**, *142*, 17782–17786.
- (7) Abdurahman, A.; Hele, T. J. H.; Gu, Q.; Zhang, J.; Peng, Q.; Zhang, M.; Friend, R. H.; Li, F.; Evans, E. W. Understanding the Luminescent Nature of Organic Radicals for Efficient Doublet Emitters and Pure-Red Light-Emitting Diodes. *Nat. Mater.* **2020**, *19*, 1224–1229.
- (8) Abella, L.; Crassous, J.; Favereau, L.; Autschbach, J. Why is the Energy of the Singly Occupied Orbital in Some Radicals below the Highest Occupied Orbital Energy? *Chem. Mater.* **2021**, *33*, 3678–3691.

- (9) Kasemthaveechok, S.; Abella, L.; Crassous, J.; Autschbach, J.; Favereau, L. Organic Radicals With Inversion of SOMO and HOMO Energies and Potential Applications in Optoelectronics. *Chem. Sci.* **2022**, *13*, 9833–9847.
- (10) Miller, J. S. Organic- and Molecule-Based Magnets. *Mater. Today* **2014**, *17*, 224–235.
- (11) Jiao, Y.; Liu, K.; Wang, G.; Wang, Y.; Zhang, X. Supramolecular Free Radicals: Near-Infrared Organic Materials with Enhanced Photothermal Conversion. *Chem. Sci.* **2015**, *6*, 3975–3980.
- (12) Jung, H. S.; Verwilt, P.; Sharma, A.; Shin, J.; Sessler, J. L.; Kim, J. S. Organic Molecule-Based Photothermal Agents: An Expanding Photothermal Therapy Universe. *Chem. Soc. Rev.* **2018**, *47*, 2280–2297.
- (13) Yang, Y.; He, P.; Wang, Y.; Bai, H.; Wang, S.; Xu, J.-F.; Zhang, X. Supramolecular Radical Anions Triggered by Bacteria *In-Situ* for Selective Photothermal Therapy. *Angew. Chem. Int. Ed.* **2017**, *56*, 16239–16242.
- (14) Xia, R.; Zheng, X.; Hu, X.; Liu, S.; Xie, Z. Photothermal-Controlled Generation of Alkyl Radical from Organic Nanoparticles for Tumor Treatment. *ACS Appl. Mater. Interfaces* **2019**, *11*, 5782–5790.
- (15) Tang, B.; Li, W.-L.; Chang, Y.; Yuan, B.; Wu, Y.; Zhang, M.-T.; Xu, J.-F.; Li, J.; Zhang, X. A Supramolecular Radical Dimer: High-Efficiency NIR-II Photothermal Conversion and Therapy. *Angew. Chem. Int. Ed.* **2019**, *58*, 15526–15531.
- (16) Peng, Q.; Obolda, A.; Zhang, M.; Li, F. Organic Light-Emitting Diodes Using a Neutral π -Radical as Emitter: The Emission from a Doublet. *Angew. Chem. Int. Ed.* **2015**, *54*, 7091–7095.
- (17) Ai, X.; Evans, E. W.; Dong, S.; Gillett, A. J.; Guo, H.; Chen, Y.; Hele, T. J.;

- Friend, R. H.; Li, F. Efficient Radical-Based Light-Emitting Diodes with Doublet Emission. *Nature* **2018**, *563*, 536–540.
- (18) Hudson, J. M.; Hele, T. J. H.; Evans, E. W. Efficient Light-Emitting Diodes from Organic Radicals with Doublet Emission. *J. Appl. Phys.* **2021**, *129*, 180901.
- (19) Slater, J. C. The Theory of Complex Spectra. *Phys. Rev.* **1929**, *34*, 1293–1322.
- (20) Li Manni, G.; Carlson, R. K.; Luo, S.; Ma, D.; Olsen, J.; Truhlar, D. G.; Gagliardi, L. Multiconfiguration Pair-Density Functional Theory. *J. Chem. Theory Comput.* **2014**, *10*, 3669–3680.
- (21) Gagliardi, L.; Truhlar, D. G.; Li Manni, G.; Carlson, R. K.; Hoyer, C. E.; Bao, J. L. Multiconfiguration Pair-Density Functional Theory: A New Way To Treat Strongly Correlated Systems. *Acc. Chem. Res.* **2017**, *50*, 66–73.
- (22) Baer, R.; Livshits, E.; Salzner, U. Tuned Range-Separated Hybrids in Density Functional Theory. *Annu. Rev. Phys. Chem.* **2010**, *61*, 85–109.
- (23) Li, Z.; Liu, W. Critical Assessment of TD-DFT for Excited States of Open-Shell Systems: I. Doublet–Doublet Transitions. *J. Chem. Theory Comput.* **2016**, *12*, 238–260.
- (24) Li, Z.; Liu, W. Critical Assessment of Time-Dependent Density Functional Theory for Excited States of Open-Shell Systems: II. Doublet-Quartet Transitions. *J. Chem. Theory Comput.* **2016**, *12*, 2517–2527.
- (25) Suo, B.; Shen, K.; Li, Z.; Liu, W. Performance of TD-DFT for Excited States of Open-Shell Transition Metal Compounds. *J. Phys. Chem. A* **2017**, *121*, 3929–3942.
- (26) Wang, Z.; Li, Z.; Zhang, Y.; Liu, W. Analytic Energy Gradients of Spin-Adapted Open-Shell Time-Dependent Density Functional Theory. *J. Chem. Phys.* **2020**, *153*, 164109.

- (27) Shao, Y.; Head-Gordon, M.; Krylov, A. I. The Spin-Flip Approach within Time-Dependent Density Functional Theory: Theory and Applications to Diradicals. *J. Chem. Phys.* **2003**, *118*, 4807–4818.
- (28) Bernard, Y. A.; Shao, Y.; Krylov, A. I. General Formulation of Spin-Flip Time-Dependent Density Functional Theory Using Non-Collinear Kernels: Theory, Implementation, and Benchmarks. *J. Chem. Phys.* **2012**, *136*, 204103.
- (29) Hait, D.; Head-Gordon, M. Highly Accurate Prediction of Core Spectra of Molecules at Density Functional Theory Cost: Attaining Sub-Electronvolt Error from a Restricted Open-Shell Kohn-Sham Approach. *J. Phys. Chem. Lett.* **2020**, *11*, 775–786.
- (30) Hait, D.; Head-Gordon, M. Excited State Orbital Optimization via Minimizing the Square of the Gradient: General Approach and Application to Singly and Doubly Excited States via Density Functional Theory. *J. Chem. Theory Comput.* **2020**, *16*, 1699–1710.
- (31) Hait, D.; Head-Gordon, M. Orbital Optimized Density Functional Theory for Electronic Excited States. *J. Phys. Chem. Lett.* **2021**, *12*, 4517–4529.
- (32) Hait, D.; Haugen, E. A.; Yang, Z.; Oosterbaan, K. J.; Leone, S. R.; Head-Gordon, M. Accurate Prediction of Core-Level Spectra of Radicals at Density Functional Theory Cost via Square Gradient Minimization and Recoupling of Mixed Configurations. *J. Chem. Phys.* **2020**, *153*, 134108.
- (33) Limacher, P. A.; Ayers, P. W.; Johnson, P. A.; De Baerdemacker, S.; Van Neck, D.; Bultinck, P. A New Mean-Field Method Suitable for Strongly Correlated Electrons: Computationally Facile Antisymmetric Products of Nonorthogonal Geminals. *J. Chem. Theory Comput.* **2013**, *9*, 1394–1401.
- (34) Sun, Q.; Yang, J.; Chan, G. K.-L. A General Second Order Complete Active Space

- Self-Consistent-Field Solver for Large-Scale Systems. *Chem. Phys. Lett.* **2017**, *683*, 291–299.
- (35) Mostafanejad, M.; DePrince, A. E. Combining Pair-Density Functional Theory and Variational Two-Electron Reduced-Density Matrix Methods. *J. Chem. Theory Comput.* **2019**, *15*, 290–302.
- (36) Hirata, S.; Lee, T. J.; Head-Gordon, M. Time-Dependent Density Functional Study on the Electronic Excitation Energies of Polycyclic Aromatic Hydrocarbon Radical Cations of Naphthalene, Anthracene, Pyrene, and Perylene. *J. Chem. Phys.* **1999**, *111*, 8904–8912.
- (37) Tokmachev, A. M.; Boggio-Pasqua, M.; Mendive-Tapia, D.; Bearpark, M. J.; Robb, M. A. Fluorescence of the Perylene Radical Cation and an Inaccessible D_0/D_1 Conical Intersection: An MMVB, RASSCF, and TD-DFT Computational Study. *J. Chem. Phys.* **2010**, *132*, 044306.
- (38) Weisman, J. L.; Lee, T. J.; Salama, F.; Head-Gordon, M. Time-dependent Density Functional Theory Calculations of Large Compact Polycyclic Aromatic Hydrocarbon Cations: Implications for the Diffuse Interstellar Bands. *Astrophys. J.* **2003**, *587*, 256–261.
- (39) Mallocci, G.; Mulas, G.; Cappellini, G.; Joblin, C. Time-Dependent Density Functional Study of the Electronic Spectra of Oligoacenes in the Charge States -1 , 0 , $+1$, and $+2$. *Chem. Phys.* **2007**, *340*, 43–58.
- (40) Bauschlicher, C. W. Time-Dependent Density Functional Theory for Polycyclic Aromatic Hydrocarbon Anions: What is the Best Approach. *Chem. Phys. Lett.* **2005**, *409*, 235–239.
- (41) Riffet, V.; Jacquemin, D.; Cauët, E.; Frison, G. Benchmarking DFT and TD-DFT

- Functionals for the Ground and Excited States of Hydrogen-Rich Peptide Radicals. *J. Chem. Theory Comput.* **2014**, *10*, 3308–3318.
- (42) Tureček, F. Benchmarking Electronic Excitation Energies and Transitions in Peptide Radicals. *J. Phys. Chem. A* **2015**, *119*, 10101–10111.
- (43) Boggio-Pasqua, M.; Bearpark, M. J. Using Density Functional Theory Based Methods to Investigate the Photophysics of Polycyclic Aromatic Hydrocarbon Radical Cations: A Benchmark Study on Naphthalene, Pyrene and Perylene Cations. *ChemPhotoChem* **2019**, *3*, 763–769.
- (44) Weisman, J. L.; Lee, T. J.; Head-Gordon, M. Electronic Spectra and Ionization Potentials of a Stable Class of Closed Shell Polycyclic Aromatic Hydrocarbon Cations. *Spectrochim. Acta A* **2001**, *57*, 931–945.
- (45) Hirata, S.; Head-Gordon, M.; Szczepanski, J.; Vala, M. Time-Dependent Density Functional Study of the Electronic Excited States of Polycyclic Aromatic Hydrocarbon Radical Ions. *J. Phys. Chem. A* **2003**, *107*, 4940–4951.
- (46) Chai, J.-D.; Head-Gordon, M. Systematic Optimization of Long-Range Corrected Hybrid Density Functionals. *J. Chem. Phys.* **2008**, *128*, 084106.
- (47) Bera, P. P.; Head-Gordon, M.; Lee, T. J. Initiating Molecular Growth in the Interstellar Medium via Dimeric Complexes of Observed Ions and Molecules. *Astron. Astrophys.* **2011**, *535*, A74.
- (48) Bera, P. P.; Head-Gordon, M.; Lee, T. J. Relative Energies, Structures, Vibrational Frequencies, and Electronic Spectra of Perylium Cation, an Oxygen-Containing Carbocyclic Ring Isoelectronic with Benzene, and its Isomers. *J. Chem. Phys.* **2013**, *139*, 174302.

- (49) Hirata, S.; Head-Gordon, M. Time-Dependent Density Functional Theory within the Tamm–Dancoff Approximation. *Chem. Phys. Lett.* **1999**, *314*, 291–299.
- (50) Becke, A. D. Density-Functional Exchange-Energy Approximation with Correct Asymptotic Behavior. *Phys. Rev. A* **1988**, *38*, 3098–3100.
- (51) Lee, C.; Yang, W.; Parr, R. G. Development of the Colle–Salvetti Correlation-Energy Formula into a Functional of the Electron Density. *Phys. Rev. B* **1988**, *37*, 785–789.
- (52) Becke, A. D. A New Mixing of Hartree–Fock and Local Density-Functional Theories. *J. Chem. Phys.* **1993**, *98*, 1372–1377.
- (53) Dreuw, A.; Head-Gordon, M. Failure of Time-Dependent Density Functional Theory for Long-Range Charge-Transfer Excited States: the Zinbacteriochlorin–Bacteriochlorin and Bacteriochlorophyll–Spheroidene Complexes. *J. Am. Chem. Soc.* **2004**, *126*, 4007–4016.
- (54) Dreuw, A.; Head-Gordon, M. Single-Eeference *Ab Initio* Methods for the Calculation of Excited States of Large Molecules. *Chem. Rev.* **2005**, *105*, 4009–4037.
- (55) Wang, Y.-L.; Wu, G.-S. Improving the TDDFT Calculation of Low-Lying Excited States for Polycyclic Aromatic Hydrocarbons Using the Tamm–Dancoff Approximation. *Int. J Quantum Chem.* **2008**, *108*, 430–439.
- (56) Hsu, C.-P.; Hirata, S.; Head-Gordon, M. Excitation Energies from Time-Dependent Density Functional Theory for Linear Polyene Oligomers: Butadiene to Decapentaene. *J. Phys. Chem. A* **2001**, *105*, 451–458.
- (57) Bauernschmitt, R.; Ahlrichs, R. Stability Analysis for Solutions of the Closed Shell Kohn–Sham Equation. *J. Chem. Phys.* **1996**, *104*, 9047–9052.
- (58) Sears, J. S.; Körzdörfer, T.; Zhang, C.-R.; Brédas, J.-L. Communication: Orbital

- Instabilities and Triplet States from Time-Dependent Density Functional Theory and Long-Range Corrected Functionals. *J. Chem. Phys.* **2011**, *135*, 151103.
- (59) Yamada, T.; Hirata, S. Singlet and Triplet Instability Theorems. *J. Chem. Phys.* **2015**, *143*, 114112.
- (60) Mallocci, G.; Joblin, C.; Mulas, G. On-Line Database of the Spectral Properties of Polycyclic Aromatic Hydrocarbons. *Chem. Phys.* **2007**, *332*, 353–359.
- (61) Mallocci, G.; Mulas, G.; Joblin, C. Electronic Absorption Spectra of PAHs Up to Vacuum UV – Towards a Detailed Model of Interstellar PAH Photophysics. *Astron. Astrophys.* **2004**, *426*, 105–117.
- (62) Rapacioli, M.; Simon, A.; Marshall, C. C. M.; Cuny, J.; Kokkin, D.; Spiegelman, F.; Joblin, C. Cationic Methylene–Pyrene Isomers and Isomerization Pathways: Finite Temperature Theoretical Studies. *J. Phys. Chem. A* **2015**, *119*, 12845–12854.
- (63) Dierksen, M.; Grimme, S. Density Functional Calculations of the Vibronic Structure of Electronic Absorption Spectra. *J. Chem. Phys.* **2004**, *120*, 3544–3554.
- (64) Dierksen, M.; Grimme, S. The Vibronic Structure of Electronic Absorption Spectra of Large Molecules: A Time-Dependent Density Functional Study on the Influence of “Exact” Hartree–Fock Exchange. *J. Phys. Chem. A* **2004**, *108*, 10225–10237.
- (65) Send, R.; Kühn, M.; Furche, F. Assessing Excited State Methods by Adiabatic Excitation Energies. *J. Chem. Theory Comput.* **2011**, *7*, 2376–2386.
- (66) Bates, J. E.; Furche, F. Harnessing the Meta-Generalized Gradient Approximation for Time-Dependent Density Functional Theory. *J. Chem. Phys.* **2012**, *137*, 164105.
- (67) Bates, J. E.; Heiche, M. C.; Liang, J.; Furche, F. Erratum: “Harnessing the Meta-Generalized Gradient Approximation for Time-Dependent Density Functional Theory” [*J. Chem. Phys.* 137, 164105 (2012)]. *J. Chem. Phys.* **2022**, *156*, 159902.

- (68) Barnes, L.; Abdul-Al, S.; Allouche, A.-R. TDDFT Assessment of Functionals for Optical 0–0 Transitions in Small Radicals. *J. Phys. Chem. A* **2014**, *118*, 11033–11046.
- (69) Perdew, J. P.; Ernzerhof, M.; Burke, K. Rationale for Mixing Exact Exchange with Density Functional Approximations. *J. Chem. Phys.* **1996**, *105*, 9982–9985.
- (70) Perdew, J. P.; Burke, K.; Ernzerhof, M. Generalized Gradient Approximation Made Simple. *Phys. Rev. Lett.* **1996**, *77*, 3865–3868.
- (71) Perdew, J. P.; Burke, K.; Ernzerhof, M. Erratum: Generalized Gradient Approximation Made Simple. *Phys. Rev. Lett.* **1997**, *78*, 1396–1396.
- (72) Adamo, C.; Barone, V. Toward Reliable Density Functional Methods without Adjustable Parameters: The PBE0 Model. *J. Chem. Phys.* **1999**, *110*, 6158–6170.
- (73) Becke, A. D. Density-Functional Thermochemistry. V. Systematic Optimization of Exchange–Correlation Functionals. *J. Chem. Phys.* **1997**, *107*, 8554–8560.
- (74) Staroverov, V. N.; Scuseria, G. E.; Tao, J.; Perdew, J. P. Comparative Assessment of a New Nonempirical Density Functional: Molecules and Hydrogen-Bonded Complexes. *J. Chem. Phys.* **2003**, *119*, 12129–12137.
- (75) Staroverov, V. N.; Scuseria, G. E.; Tao, J.; Perdew, J. P. Erratum: “Comparative Assessment of a New Nonempirical Density Functional: Molecules and Hydrogen-Bonded Complexes” [J. Chem. Phys. 119, 12129 (2003)]. *J. Chem. Phys.* **2004**, *121*, 11507–11507.
- (76) Zhao, Y.; Truhlar, D. G. Exploring the Limit of Accuracy of the Global Hybrid Meta Density Functional for Main-Group Thermochemistry, Kinetics, and Noncovalent Interactions. *J. Chem. Theory Comput.* **2008**, *4*, 1849–1868.
- (77) Zhao, Y.; Truhlar, D. G. The M06 Suite of Density Functionals for Main Group Thermochemistry, Thermochemical Kinetics, Noncovalent Interactions, Excited States, and

- Transition Elements: Two New Functionals and Systematic Testing of Four M06-Class Functionals and 12 Other Functionals. *Theor. Chem. Acc.* **2008**, *120*, 215–241.
- (78) Chai, J.-D.; Head-Gordon, M. Long-Range Corrected Hybrid Density Functionals with Damped Atom–Atom Dispersion Corrections. *Phys. Chem. Chem. Phys.* **2008**, *10*, 6615–6620.
- (79) Lin, Y.-S.; Li, G.-D.; Mao, S.-P.; Chai, J.-D. Long-Range Corrected Hybrid Density Functionals with Improved Dispersion Corrections. *J. Chem. Theory Comput.* **2013**, *9*, 263–272.
- (80) Mardirossian, N.; Head-Gordon, M. ω B97X-V: A 10-Parameter, Range-Separated Hybrid, Generalized Gradient Approximation Density Functional with Nonlocal Correlation, Designed by a Survival-of-the-Fittest Strategy. *Phys. Chem. Chem. Phys.* **2014**, *16*, 9904–9924.
- (81) Henderson, T. M.; Janesko, B. G.; Scuseria, G. E. Generalized Gradient Approximation Model Exchange Holes for Range-Separated Hybrids. *J. Chem. Phys.* **2008**, *128*, 194105.
- (82) Heyd, J.; Scuseria, G. E.; Ernzerhof, M. Hybrid Functionals Based on a Screened Coulomb Potential. *J. Chem. Phys.* **2003**, *118*, 8207–8215.
- (83) Krukau, A. V.; Vydrov, O. A.; Izmaylov, A. F.; Scuseria, G. E. Influence of the Exchange Screening Parameter on the Performance of Screened Hybrid Functionals. *J. Chem. Phys.* **2006**, *125*, 224106.
- (84) Rohrdanz, M. A.; Herbert, J. M. Simultaneous Benchmarking of Ground- and Excited-State Properties with Long-Range-Corrected Density Functional Theory. *J. Chem. Phys.* **2008**, *129*, 034107.

- (85) Rohrdanz, M. A.; Martins, K. M.; Herbert, J. M. A Long-Range-Corrected Density Functional that Performs Well for Both Ground-State Properties and Time-Dependent Density Functional Theory Excitation Energies, Including Charge-Transfer Excited States. *J. Chem. Phys.* **2009**, *130*, 054112.
- (86) Mardirossian, N.; Head-Gordon, M. ω B97M-V: A Combinatorially Optimized, Range-Separated Hybrid, *meta*-GGA Density Functional with VV10 Nonlocal Correlation. *J. Chem. Phys.* **2016**, *144*, 214110.
- (87) Zhang, Y.; Xu, X.; Goddard, W. A. Doubly Hybrid Density Functional for Accurate Descriptions of Nonbond Interactions, Thermochemistry, and Thermochemical Kinetics. *Proc. Natl. Acad. Sci.* **2009**, *106*, 4963–4968.
- (88) Lin, Z.; Van Voorhis, T. Triplet Tuning: A Novel Family of Non-Empirical Exchange–Correlation Functionals. *J. Chem. Theory Comput.* **2019**, *15*, 1226–1241.
- (89) Ju, C.-W.; French, E. J.; Geva, N.; Kohn, A. W.; Lin, Z. Stacked Ensemble Machine Learning for Range-Separation Parameters. *J. Phys. Chem. Lett.* **2021**, *12*, 9516–9524.
- (90) Wolpert, D. H. Stacked Generalization. *Neural Netw.* **1992**, *5*, 241–259.
- (91) Polikar, R. Ensemble Based Systems in Decision Making. *IEEE Circuits Syst. Mag.* **2006**, *6*, 21–45.
- (92) Rokach, L. Ensemble-Based Classifiers. *Artif. Intell. Rev.* **2010**, *33*, 1–39.
- (93) Opitz, D.; Maclin, R. Popular Ensemble Methods: An Empirical Study. *J. Artif. Intell. Res.* **1999**, *11*, 169–198.
- (94) Coscrato, V.; de Almeida Inácio, M. H.; Izbicki, R. The NN-Stacking: Feature Weighted Linear Stacking through Neural Networks. *Neurocomputing* **2020**, *399*, 141–152.

- (95) Breiman, L. Stacked Regressions. *Mach. Learn.* **1996**, *24*, 49–64.
- (96) Yang, Q.; Li, Y.; Yang, J.-D.; Liu, Y.; Zhang, L.; Luo, S.; Cheng, J.-P. Holistic Prediction of the pK_a in Diverse Solvents Based on a Machine-Learning Approach. *Angew. Chem. Int. Ed.* **2020**, *59*, 19282–19291.
- (97) Rogers, D.; Hahn, M. Extended-Connectivity Fingerprints. *J. Chem. Inf. Model.* **2010**, *50*, 742–754.
- (98) Willighagen, E. L.; Mayfield, J. W.; Alvarsson, J.; Berg, A.; Carlsson, L.; Jelizkova, N.; Kuhn, S.; Pluskal, T.; Rojas-Chertó, M.; Spjuth, O. et al. The Chemistry Development Kit (CDK) v2.0: Atom Typing, Depiction, Molecular Formulas, and Substructure Searching. *J. Cheminf.* **2017**, *9*, 1–19.
- (99) Grimme, S.; Bannwarth, C.; Shushkov, P. A Robust and Accurate Tight-Binding Quantum Chemical Method for Structures, Vibrational Frequencies, and Noncovalent Interactions of Large Molecular Systems Parametrized for All *spd*-Block Elements ($Z = 1 - 86$). *J. Chem. Theory Comput.* **2017**, *13*, 1989–2009.
- (100) Bannwarth, C.; Ehlert, S.; Grimme, S. GFN2-xTB—An Accurate and Broadly Parametrized Self-Consistent Tight-Binding Quantum Chemical Method with Multipole Electrostatics and Density-Dependent Dispersion Contributions. *J. Chem. Theory Comput.* **2019**, *15*, 1652–1671.
- (101) Pracht, P.; Caldeweyher, E.; Ehlert, S.; Grimme, S. A Robust Non-Self-Consistent Tight-Binding Quantum Chemistry Method for Large Molecules. *ChemRxiv* **2019**, doi: 10.26434/chemrxiv.8326202.v1.
- (102) Koopmans, T. Über die Zuordnung von Wellenfunktionen und Eigenwerten zu den Einzelnen Elektronen Eines Atoms. *Physica* **1934**, *1*, 104–113.

- (103) Kronik, L.; Stein, T.; Refaely-Abramson, S.; Baer, R. Excitation Gaps of Finite-Sized Systems from Optimally Tuned Range-Separated Hybrid Functionals. *J. Chem. Theory Comput.* **2012**, *8*, 1515–1531.
- (104) Livshits, E.; Baer, R. A Well-Tempered Density Functional Theory of Electrons in Molecules. *Phys. Chem. Chem. Phys.* **2007**, *9*, 2932–2941.
- (105) Stein, T.; Kronik, L.; Baer, R. Reliable Prediction of Charge Transfer Excitations in Molecular Complexes Using Time-Dependent Density Functional Theory. *J. Am. Chem. Soc.* **2009**, *131*, 2818–2820.
- (106) Stein, T.; Eisenberg, H.; Kronik, L.; Baer, R. Fundamental Gaps in Finite Systems from Eigenvalues of a Generalized Kohn–Sham Method. *Phys. Rev. Lett.* **2010**, *105*, 266802.
- (107) Kuritz, N.; Stein, T.; Baer, R.; Kronik, L. Charge-Transfer-Like $\pi \rightarrow \pi^*$ Excitations in Time-Dependent Density Functional Theory: A Conundrum and Its Solution. *J. Chem. Theory Comput.* **2011**, *7*, 2408–2415.
- (108) Perdew, J. P.; Burke, K.; Ernzerhof, M. Generalized Gradient Approximation Made Simple. *Phys. Rev. Lett.* **1996**, *77*, 3865.
- (109) Yanai, T.; Tew, D. P.; Handy, N. C. A New Hybrid Exchange–Correlation Functional Using the Coulomb-Attenuating Method (CAM-B3LYP). *Chem. Phys. Lett.* **2004**, *393*, 51–57.
- (110) Gong, J.; Lam, J. W. Y.; Tang, B. Z. Benchmark and Parameter Tuning of Hybrid Functionals for Fast Calculation of Excitation Energies of AIEgens. *Phys. Chem. Chem. Phys.* **2020**, *22*, 18035–18039.
- (111) Ali, A.; Rafiq, M. I.; Zhang, Z.; Cao, J.; Geng, R.; Zhou, B.; Tang, W. TD-DFT

- Benchmark for UV-Visible Spectra of Fused-Ring Electron Acceptors Using Global and Range-Separated Hybrids. *Phys. Chem. Chem. Phys.* **2020**, *22*, 7864–7874.
- (112) Alipour, M.; Safari, Z. Photophysics of OLED Materials with Emitters Exhibiting Thermally Activated Delayed Fluorescence and Used in Hole/Electron Transporting Layer from Optimally Tuned Range-Separated Density Functional Theory. *J. Phys. Chem. C* **2018**, *123*, 746–761.
- (113) Bejarano, F.; Olavarria-Contreras, I. J.; Droghetti, A.; Rungger, I.; Rudnev, A.; Gutiérrez, D.; Mas-Torrent, M.; Veciana, J.; van der Zant, H. S. J.; Rovira, C. et al. Robust Organic Radical Molecular Junctions Using Acetylene Terminated Groups for C–Au Bond Formation. *J. Am. Chem. Soc.* **2018**, *140*, 1691–1696.
- (114) Hattori, Y.; Kusamoto, T.; Sato, T.; Nishihara, H. Synergistic Luminescence Enhancement of a Pyridyl-Substituted Triarylmethyl Radical Based on Fluorine Substitution and Coordination to Gold. *Chem. Commun.* **2016**, *52*, 13393–13396.
- (115) Ai, X.; Chen, Y.; Feng, Y.; Li, F. A Stable Room-Temperature Luminescent Biphenylmethyl Radical. *Angew. Chem. Int. Ed.* **2018**, *57*, 2869–2873.
- (116) Dong, S.; Xu, W.; Guo, H.; Yan, W.; Zhang, M.; Li, F. Effects of Substituents on Luminescent Efficiency of Stable Triaryl Methyl Radicals. *Phys. Chem. Chem. Phys.* **2018**, *20*, 18657–18662.
- (117) Abdurahman, A.; Chen, Y.; Ai, X.; Ablikim, O.; Gao, Y.; Dong, S.; Li, B.; Yang, B.; Zhang, M.; Li, F. A Pure Red Luminescent β -Carboline-Substituted Biphenylmethyl Radical: Photophysics, Stability and OLEDs. *J. Mater. Chem. C* **2018**, *6*, 11248–11254.
- (118) Rösel, S.; Becker, J.; Allen, W. D.; Schreiner, P. R. Probing the Delicate Balance between Pauli Repulsion and London Dispersion with Triphenylmethyl Derivatives. *J. Am. Chem. Soc.* **2018**, *140*, 14421–14432.

- (119) Fischer, H.; Baer, R.; Hany, R.; Verhoolen, I.; Walbiner, M. 2,2-Dimethoxy-2-Phenylacetophenone: Photochemistry and Free Radical Photofragmentation. *J. Chem. Soc., Perkin Trans. 2* **1990**, 787–798.
- (120) López, M.; Velasco, D.; López-Calahorra, F.; Juliá, L. Light-Emitting Persistent Radicals for Efficient Sensor Devices of Solvent Polarity. *Tetrahedron Lett.* **2008**, *49*, 5196–5199.
- (121) Gao, Y.; Xu, W.; Ma, H.; Obolda, A.; Yan, W.; Dong, S.; Zhang, M.; Li, F. Novel Luminescent Benzimidazole-Substituent Tris(2,4,6-Trichlorophenyl)methyl Radicals: Photophysics, Stability, and Highly Efficient Red-Orange Electroluminescence. *Chem. Mater.* **2017**, *29*, 6733–6739.
- (122) Wu, X.; Kim, J. O.; Medina, S.; Ramírez, F. J.; Mayorga Burrezo, P.; Wu, S.; Lim, Z. L.; Lambert, C.; Casado, J.; Kim, D. et al. Push–Pull-Type Polychlorotriphenylmethyl Radicals: New Two-Photon Absorbers and Dyes for Generation of Photo-Charges. *Chem. Eur. J.* **2017**, *23*, 7698–7702.
- (123) Gu, X.; Gopalakrishna, T. Y.; Phan, H.; Ni, Y.; Herng, T. S.; Ding, J.; Wu, J. A Three-Dimensionally π -Conjugated Diradical Molecular Cage. *Angew. Chem. Int. Ed.* **2017**, *56*, 15383–15387.
- (124) Heckmann, A.; Lambert, C.; Goebel, M.; Wortmann, R. Synthesis and Photophysics of a Neutral Organic Mixed-Valence Compound. *Angew. Chem. Int. Ed.* **2004**, *43*, 5851–5856.
- (125) Ballester, M.; Riera, J.; Castaner, J.; Rodriguez, A.; Rovira, C.; Veciana, J. Inert Carbon Free Radicals. 3. Monofunctionalized Radicals From Perchlorotriphenylcarbenium Hexachloroantimonate. *J. Org. Chem.* **1982**, *47*, 4498–4505.
- (126) Bonvoisin, J.; Launay, J.-P.; Rovira, C.; Veciana, J. Purely Organic Mixed-Valence Molecules with Nanometric Dimensions Showing Long-Range Electron Transfer.

- Synthesis, and Optical and EPR Studies of a Radical Anion Derived from a Bis(Triarylmethyl)Diradical. *Angew. Chem. Int. Ed.* **1994**, *33*, 2106–2109.
- (127) Teruel, L.; Viadel, L.; Carilla, J.; Fajarí, L.; Brillas, E.; Sañé, J.; Rius, J.; Juliá, L. (4-Amino-2, 6-Dichlorophenyl)-bis (2, 4, 6-Trichlorophenyl) Methyl Radical: A New Constituent of Organic Magnetic Materials. *J. Org. Chem.* **1996**, *61*, 6063–6066.
- (128) Neckers, D.; Rajadurai, S.; Valdes-Aguilera, O.; Zakrzewski, A.; Linden, S. Photophysics and Photochemistry of P-Benzoylphenyldiphenylmethyl in Solution. *Tetrahedron Lett.* **1988**, *29*, 5109–5112.
- (129) Ruberu, S. R.; Fox, M. A. Photochemical Behavior of Stable Free Radicals: The Photochemistry of Perchlorodiphenylmethyl Radical. *J. Phys. Chem.* **1993**, *97*, 143–149.
- (130) Peng, Q.; Obolda, A.; Zhang, M.; Li, F. Organic Light-Emitting Diodes Using a Neutral π Radical as Emitter: The Emission from a Doublet. *Angew. Chem. Int. Ed.* **2015**, *54*, 7091–7095.
- (131) Cui, Z.; Ye, S.; Wang, L.; Guo, H.; Obolda, A.; Dong, S.; Chen, Y.; Ai, X.; Abdurahman, A.; Zhang, M. et al. Radical-Based Organic Light-Emitting Diodes with Maximum External Quantum Efficiency of 10.6%. *J. Phys. Chem. Lett.* **2018**, *9*, 6644–6648.
- (132) Jin, Q.; Chen, S.; Sang, Y.; Guo, H.; Dong, S.; Han, J.; Chen, W.; Yang, X.; Li, F.; Duan, P. Circularly Polarized Luminescence of Achiral Open-Shell π -Radicals. *Chem. Commun.* **2019**, *55*, 6583–6586.
- (133) Hattori, Y.; Kusamoto, T.; Nishihara, H. Highly Photostable Luminescent Open-Shell (3,5-Dihalo-4-Pyridyl)bis(2,4,6-Trichlorophenyl)Methyl Radicals: Significant Effects of Halogen Atoms on Their Photophysical and Photochemical Properties. *RSC Adv.* **2015**, *5*, 64802–64805.

- (134) Uchida, K.; Mou, Z.; Kertesz, M.; Kubo, T. Fluxional σ -Bonds of the 2,5,8-Trimethylphenalenyl Dimer: Direct Observation of the Sixfold σ -Bond Shift via a π -Dimer. *J. Am. Chem. Soc.* **2016**, *138*, 4665–4672.
- (135) Small, D.; Zaitsev, V.; Jung, Y.; Rosokha, S. V.; Head-Gordon, M.; Kochi, J. K. Intermolecular π -to- π Bonding between Stacked Aromatic Dyads. Experimental and Theoretical Binding Energies and Near-IR Optical Transitions for Phenalenyl Radical/Radical versus Radical/Cation Dimerizations. *J. Am. Chem. Soc.* **2004**, *126*, 13850–13858.
- (136) Patrascu, B.; Lete, C.; Popescu, C.; Matache, M.; Paun, A.; Madalan, A.; Ionitaa, P. Synthesis and Spectral Comparison of Electronic and Molecular Properties of Some Hydrazines and Hydrazyl Free Radicals. *Arkivoc* **2020**, *2020*, 1–10.
- (137) Miura, Y.; Tanaka, A.; Hirotsu, K. ESR Studies of Nitrogen-Centered Free Radicals. 40. Exceptionally Persistent Nitrogen-Centered Free Radicals. Preparation, Isolation, and Molecular Structure of N-(Arylthio)-2,4, 6-Triphenylanilino Radicals. *J. Org. Chem.* **1991**, *56*, 6638–6643.
- (138) Miura, Y.; Yamamoto, A.; Katsura, Y.; Kinoshita, M.; Sato, S.; Tamura, C. ESR Studies of Nitrogen-Centered Free Radicals. 17. [(4-Nitrophenyl)Thio](2,4, 6-Tri-Tert-Butylphenyl)Aminyl: Its Preparation, Isolation, and Molecular Structure. *J. Org. Chem.* **1982**, *47*, 2618–2622.
- (139) Miura, Y.; Yamamoto, A.; Katsura, Y.; Kinoshita, M. ESR Study of Persistent Thioaminyls, N-(Arylthio)-3,5-Di-Tert-Butylphenylaminyls. *J. Org. Chem.* **1980**, *45*, 3875–3880.
- (140) Miura, Y.; Tomimura, T. First Isolation of N-Alkoxyaminyl Radicals. *Chem. Commun.* **2001**, 627–628.

- (141) Fabian, J.; Decker, D.; Mayer, R. Formation and Properties of *N*-Arylthioaminyls. *Zeitschrift fur Chemie* **1988**, *28*, 325–326.
- (142) Levin, P. P.; Kokrashvili, T. A.; Kuz'min, V. A. Effect of Solvent and Substituents on Electron and Hydrogen Atom Transfer in Quenching of Quinone Triplets by Secondary Aromatic Amines. *Bulletin of the Academy of Sciences of the USSR, Division of Chemical Science* **1983**, *32*, 251–257.
- (143) Miura, Y.; Tomimura, T.; Teki, Y. Heterocycle-Substituted Stable Thioaminyl Radicals: Isolation, ESR Spectra, and Magnetic Properties. *J. Org. Chem.* **2000**, *65*, 7889–7895.
- (144) Ionita, G.; Căproiu, M. T.; Meghea, A.; Maior, O.; Rovinaru, M.; Ioniță, P. Synthesis Based on 9-Amino-N-Picrylcarbazyll. *Pol. J. Chem.* **1999**, *73*, 1177–1183.
- (145) Symons, M. C. R.; Pena-Nuñez, A. S. Solvation of Nitroxides. *J. Chem. Soc., Faraday Trans. 1* **1985**, *81*, 2421–2435.
- (146) Imino- and Bis-Imino-Pyridines With *N*-Ter-Butyl-*N*-Aminoxyll Group: Synthesis, Oxidation and Use As Ligand Towards M_2^+ (Mn, Ni, Zn) and Gd_3^+ . *J. Organomet. Chem.* **2005**, *690*, 197–210.
- (147) Golubev, V. A.; Sen', V. D. Mechanism of Autoreduction of Bis(4-Methoxyphenyl)-Oxoammonium Perchlorate in Aqueous Alkali. *Russ. J. Org. Chem.* **2011**, *47*, 1313–1317.
- (148) Oka, H.; Tamura, T.; Miura, Y.; Teki, Y. Synthesis and Magnetic Behaviour of Poly(1,3-Phenylene)-Based Polyradical Carrying *N*-Tert-Butylaminoxyll Radicals. *J. Mater. Chem.* **1999**, *9*, 1227–1232.
- (149) Sueishi, Y.; Yoshioka, C.; Takemoto, K.; Kotake, Y. An Optical Spectroscopic Study

- on Carbon–And Oxygen-Centered Free Radical Adducts Trapped by a Bi-Functional Nitrene Spin Trap. *Zeitschrift fur Physikalische Chemie* **2002**, *216*, 1353 – 1360.
- (150) Sasaki, S.; Kato, K.; Yoshifuji, M. Synthesis and Redox Properties of Crowded Triarylyphosphines Carrying a Nitroxide Radical and Related Compounds. *Bull. Chem. Soc. Jpn.* **2007**, *80*, 1791–1798.
- (151) Kigoshi, M.; Sato, K.; Niki, E. Oxidation of Lipids Induced by Dioctadecyl Hyponitrite and Di-*t*-Butyl Hyponitrite in Organic Solution and in Aqueous Dispersions. Effects of Reaction Medium and Size of Radicals on Efficiency of Chain Initiation. *Bull. Chem. Soc. Jpn.* **1993**, *66*, 2954–2959.
- (152) Grabner, G.; Koehler, G.; Marconi, G.; Monti, S.; Venuti, E. Photophysical Properties of Methylated Phenols in Nonpolar Solvents. *J. Phys. Chem.* **1990**, *94*, 3609–3613.
- (153) Modarelli, D. A.; Rossitto, F. C.; Lahti, P. M. Convenient Unimolecular Sources of Aryloxy Radicals I – Aryloxyoxalyl Chlorides. *Tetrahedron Lett.* **1989**, *30*, 4473–4476.
- (154) Ouchi, A.; Nagaoka, S.-I.; Mukai, K. Tunneling Effect in Regeneration Reaction of Vitamin E by Ubiquinol. *J. Phys. Chem. B* **2010**, *114*, 6601–6607.
- (155) Roginskii, V. A.; Dubinskii, V. Z.; Miller, V. B. Dissociation of 4-Tert-Butoxy-2, 6-Di-Tertbutylphenoxy and Antioxid Active Activity of Phenols with Alkokoxy Substituents. *Bulletin of the Academy of Sciences of the USSR, Division of Chemical Science* **1981**, *30*, 2341–2344.
- (156) Orio, M.; Jarjayes, O.; Baptiste, B.; Philouze, C.; Duboc, C.; Mathias, J.-L.; Benisvy, L.; Thomas, F. Geometric and Electronic Structures of Phenoxy Radicals Hydrogen Bonded to Neutral and Cationic Partners. *Chem. Eur. J.* **2012**, *18*, 5416–5429.

- (157) Rausch, R.; Schmidt, D.; Bialas, D.; Krummenacher, I.; Braunschweig, H.; Würthner, F. Stable Organic (Bi)Radicals by Delocalization of Spin Density into the Electron-Poor Chromophore Core of Isoindigo. *Chem. Eur. J.* **2018**, *24*, 3420–3424.
- (158) Mitsuoka, M.; Sakamaki, D.; Fujiwara, H. Tetrathiafulvalene-Inserted Diphenoquinone: Synthesis, Structure, and Dynamic Redox Property. *Chem. Eur. J.* **2020**, *26*, 14144–14151.
- (159) Hachmann, J.; Olivares-Amaya, R.; Atahan-Evrenk, S.; Amador-Bedolla, C.; Sánchez-Carrera, R. S.; Gold-Parker, A.; Vogt, L.; Brockway, A. M.; Aspuru-Guzik, A. The Harvard Clean Energy Project: Large-Scale Computational Screening and Design of Organic Photovoltaics on the World Community Grid. *J. Phys. Chem. Lett.* **2011**, *2*, 2241–2251.
- (160) Hachmann, J.; Olivares-Amaya, R.; Jinich, A.; Appleton, A. L.; Blood-Forsythe, M. A.; Seress, L. R.; Román-Salgado, C.; Trepte, K.; Atahan-Evrenk, S.; Er, S. et al. Lead Candidates for High-Performance Organic Photovoltaics from High-Throughput Quantum Chemistry—the Harvard Clean Energy Project. *Energy Environ. Sci.* **2014**, *7*, 698–704.
- (161) Ramsundar, B.; Eastman, P.; Walters, P.; Pande, V. *Deep Learning for the Life Sciences: Applying Deep Learning to Genomics, Microscopy, Drug Discovery, and More*; O’Reilly Media, 2019.
- (162) Ju, C.-W.; Bai, H.; Li, B.; Liu, R. Machine Learning Enables Highly Accurate Predictions of PhotoPhysical Properties of Organic Fluorescent Materials: Emission Wavelengths and Quantum Yields. *J. Chem. Inf. Model.* **2021**, *61*, 1053–1065.
- (163) Lopez, S. A.; Pyzer-Knapp, E. O.; Simm, G. N.; Lutzow, T.; Li, K.; Seress, L. R.; Hachmann, J.; Aspuru-Guzik, A. The Harvard Organic Photovoltaic Dataset. *Sci. Data* **2016**, *3*, 160086.

- (164) Gómez-Bombarelli, R.; Aguilera-Iparraguirre, J.; Hirzel, T. D.; Duvenaud, D.; Maclaurin, D.; Blood-Forsythe, M. A.; Chae, H. S.; Einzinger, M.; Ha, D.-G.; Wu, T. et al. Design of Efficient Molecular Organic Light-Emitting Diodes by a High-Throughput Virtual Screening and Experimental Approach. *Nat. Mater.* **2016**, *15*, 1120–1127.
- (165) Tibshirani, R. Regression Shrinkage and Selection via the Lasso. *J. R. Stat. Soc. Series B Stat. Methodol.* **1996**, *58*, 267–288.
- (166) Chen, T.; Guestrin, C. XgBoost: A Scalable Tree Boosting System. Proceedings of the 22nd ACM SIGKDD International Conference on Knowledge Discovery and Data Mining. 2016; pp 785–794.
- (167) Ke, G.; Meng, Q.; Finley, T.; Wang, T.; Chen, W.; Ma, W.; Ye, Q.; Liu, T.-Y. LightGBM: A Highly Efficient Gradient Boosting Decision Tree. *Adv. Neural Inf. Process. Syst.* **2017**, *30*, 3146–3154.
- (168) Friedman, J. H. Stochastic Gradient Boosting. *Comput. Stat. Data Anal.* **2002**, *38*, 367–378.
- (169) Ho, T. K. Random Decision Forests. Proceedings of 3rd International Conference on Document Analysis and Recognition. 1995; pp 278–282.
- (170) Vovk, V. Kernel Ridge Regression. In *Empirical Inference: Festschrift in Honor of Vladimir N. Vapnik*; Schölkopf, B., Luo, Z., Vovk, V., Eds.; Springer Berlin Heidelberg: Berlin, Heidelberg, 2013; pp 105–116.
- (171) Cortes, C.; Vapnik, V. Support-Vector Networks. *Mach. Learn.* **1995**, *20*, 273–297.
- (172) Balabin, R. M.; Lomakina, E. I. Support Vector Machine Regression (LS-SVM)—An Alternative to Artificial Neural Networks (ANNs) for the Analysis of Quantum Chemistry Data? *Phys. Chem. Chem. Phys.* **2011**, *13*, 11710–11718.

- (173) Kamath, A.; Vargas-Hernández, R. A.; Krems, R. V.; Carrington, T.; Manzhos, S. Neural Networks vs Gaussian Process Regression for Representing Potential Energy Surfaces: A Comparative Study of Fit Quality and Vibrational Spectrum Accuracy. *J. Chem. Phys.* **2018**, *148*, 241702.
- (174) Zhou, Y.; Wu, J.; Chen, S.; Chen, G. Toward the Exact Exchange–Correlation Potential: A Three-Dimensional Convolutional Neural Network Construct. *J. Phys. Chem. Lett.* **2019**, *10*, 7264–7269.
- (175) Sun, W.; Zheng, Y.; Yang, K.; Zhang, Q.; Shah, A. A.; Wu, Z.; Sun, Y.; Feng, L.; Chen, D.; Xiao, Z. et al. Machine Learning-Assisted Molecular Design and Efficiency Prediction for High-Performance Organic Photovoltaic Materials. *Sci. Adv.* **2019**, *5*, eaay4275.
- (176) Meftahi, N.; Klymenko, M.; Christofferson, A. J.; Bach, U.; Winkler, D. A.; Russo, S. P. Machine Learning Property Prediction for Organic Photovoltaic Devices. *Npj Comput. Mater.* **2020**, *6*, 166.
- (177) Mahmood, A.; Wang, J.-L. Machine Learning for High Performance Organic Solar Cells: Current Scenario and Future Prospects. *Energy Environ. Sci.* **2021**, *14*, 90–105.
- (178) Jiang, D.; Wu, Z.; Hsieh, C.-Y.; Chen, G.; Liao, B.; Wang, Z.; Shen, C.; Cao, D.; Wu, J.; Hou, T. Could Graph Neural Networks Learn Better Molecular Representation for Drug Discovery? A Comparison Study of Descriptor-Based and Graph-Based Models. *J. Cheminformatics* **2021**, *13*, 1–23.
- (179) Fabregat, R.; Fabrizio, A.; Engel, E. A.; Meyer, B.; Juraskova, V.; Ceriotti, M.; Corminboeuf, C. Local Kernel Regression and Neural Network Approaches to the Conformational Landscapes of Oligopeptides. *J. Chem. Theory Comput.* **2022**, *18*, 1467–1479.

- (180) Efron, B.; Hastie, T.; Johnstone, I.; Tibshirani, R. Least Angle Regression. *Ann. Statist.* **2004**, *32*, 407–499.
- (181) Hinton, G. E.; Roweis, S. Stochastic Neighbor Embedding. *Advances in Neural Information Processing Systems*. 2002.
- (182) Glem, R. C.; Bender, A.; Arnby, C. H.; Carlsson, L.; Boyer, S.; Smith, J. Circular Fingerprints: Flexible Molecular Descriptors with Applications from Physical Chemistry to ADME. *IDrugs* **2006**, *9*, 199–204.
- (183) Yap, C. W. PaDEL-Descriptor: An Open Source Software to Calculate Molecular Descriptors and Fingerprints. *J. Comput. Chem.* **2011**, *32*, 1466–1474.
- (184) Cheng, L.; Sun, J.; Miller, T. F. I. Accurate Molecular-Orbital-Based Machine Learning Energies via Unsupervised Clustering of Chemical Space. *J. Chem. Theory Comput.* **2022**, *18*, 4826–4835.
- (185) Townsend, J.; Micucci, C. P.; Hymel, J. H.; Maroulas, V.; Vogiatzis, K. D. Representation of Molecular Structures with Persistent Homology for Machine Learning Applications in Chemistry. *Nat. Comm.* **2020**, *11*, 3230.
- (186) Janet, J. P.; Duan, C.; Nandy, A.; Liu, F.; Kulik, H. J. Navigating Transition-Metal Chemical Space: Artificial Intelligence for First-Principles Design. *Acc. Chem. Res.* **2021**, *54*, 532–545.
- (187) Janet, J. P.; Kulik, H. J. Resolving Transition Metal Chemical Space: Feature Selection for Machine Learning and Structure–Property Relationships. *J. Phys. Chem. A* **2017**, *121*, 8939–8954.
- (188) Naveja, J. J.; Medina-Franco, J. L. Finding Constellations in Chemical Space Through Core Analysis. *Front. Chem.* **2019**, *7*.

- (189) Cohen, A. J.; Mori-Sánchez, P.; Yang, W. Challenges for Density Functional Theory. *Chem. Rev.* **2012**, *112*, 289–320.
- (190) Reuther, A.; Kepner, J.; Byun, C.; Samsi, S.; Arcand, W.; Bestor, D.; Bergeron, B.; Gadepally, V.; Houle, M.; Hubbell, M. et al. Interactive Supercomputing on 40,000 Cores for Machine Learning and Data Analysis. 2018 IEEE High Performance Extreme Computing Conference (HPEC). 2018; pp 1–6.